

A Highly Efficient Bi-based Electrocatalyst for the Reduction of CO₂ to Formate

Luyu Shao¹, Weixin Lv^{2,*}, Rui Zhang², Fenyong Kong², Lanzi Cheng¹, Wei Wang^{2,*}

¹ School of Chemistry and Chemical Engineering, Jiangsu University, Zhenjiang 212013, P. R. China

² School of Chemistry and Chemical Engineering, Yancheng Institute of Technology, Yancheng 224051, P. R. China

*E-mail: weixin841230@163.com (W.X. Lv); wangw@ycit.edu.cn (W. Wang).

Received: 5 September 2018 / Accepted: 23 October 2018 / Published: 30 November 2018

The electrochemical reduction of carbon dioxide (CO₂) has received significant attention as a viable man-made carbon cycle able to replenish the natural carbon cycle. Although Bi-based materials are promising catalysts for the reduction of CO₂ to formate, the effects of the morphology and the structure of these materials on their properties remain unclear. In this work, a nano Bi₂O₂CO₃ (BOC) material was synthesized and subsequently calcined at 300, 400, and 500 °C to form three different Bi₂O₃ samples namely, Bi₂O₃-1, Bi₂O₃-2, and Bi₂O₃-3, respectively. Both the BOC and the calcined materials were decorated on glassy carbon electrodes and then reduced to metallic Bi to form r-BOC, r-Bi₂O₃-1, r-Bi₂O₃-2, and r-Bi₂O₃-3 samples. We compared the performance of the four reduced Bi-based catalysts towards the reduction of CO₂ in an attempt to study the structure–activity relationship of Bi-based catalysts. r-Bi₂O₃-3 showed excellent catalytic performance towards the reduction of CO₂ reduction to formate. Thus, this catalyst showed a faradaic efficiency (FE) for the electrochemical reduction of CO₂ to formate as high as 95% at an overpotential of 0.99 V and with a current density of 17 mA cm⁻². r-Bi₂O₃-3 outperformed the rest of the reduced samples and most of the catalysts reported in the literature.

Keywords: Carbon dioxide; Electrochemical reduction; Formate; Metal bismuth; Structure–activity relationship.

1. INTRODUCTION

With the beginning of the industry era, massive amounts of carbon dioxide (CO₂) were generated by human activities. According to recent reports [1], the level of CO₂ in the atmosphere is increasing at an alarming rate of 2 ppm per year, and the current CO₂ concentration in the atmosphere reaches 411 ppm [2]. This large concentration of CO₂ in the atmosphere produces severe carbon imbalances on the

planet, generating a passive influence on our living environment by global warming-related issues such as glacier melting, ocean acidification, and land desertification [3].

Therefore, there is an urgent need for developing strategies able to reduce global CO₂ concentrations such as CO₂ capture and sequestration (CCS) and the conversion of CO₂ into useful fuels [4]. While capture and storage technologies can reduce emissions, they require energy to capture and transport the CO₂, and there is always the risk of a sudden leak [5]. These technologies do not solve the problem of the large-scale use of non-renewable fossil fuels and this strategy cannot fundamentally solve the greenhouse effect in the short-term. Therefore, other technologies are required to complement CCS and convert CO₂ into useful fuels. In this sense, photocatalysis, photoelectrocatalysis, and electrochemical reduction, among others are receiving increasing attention from the researchers [6–9].

Among these pathways, electrochemical reduction of CO₂ is particularly popular and has achieved significant progresses in recent decades. The electrochemical reduction of CO₂ is expected to overcome certain challenges since it allows to effectively convert electric energy into high-energy-density fuels for storage [9]. Thus, electrochemical reduction can reduce CO₂ emissions while effectively converting CO₂ into higher value chemicals such as carbon monoxide, methanol, ethanol, syngas, and formate/formic acid (depending on the pH, “formate” is used hereafter for both forms) at an ambient temperature and pressure [9–12]. Among all the potential products, formate is an excellent target for CO₂ electrochemical reduction. Preliminary studies on the electrochemical reduction of CO₂ to formate in aqueous solution were published in 1870 [13]. Formate is an important feedstock used in numerous chemical industries as pharmaceutical precursor, crop protection, leather tanning, electrowinning, and aircraft deicing agents [14–16]. In addition, formate is considered to be a good hydrogen storage material for direct formic acid fuel cells in virtue of its high volumetric capacity (53 g H₂ L⁻¹) [17, 18]. In this sense, Agarwal et al. suggested that formate is the most interesting product for the large-scale electrochemical reduction of CO₂ from the engineering and economic points of view, being operationally profitable compared to other electroreduction products [19].

Several metals such as Pb, In, Ir, Cu, Sn, and especially Bi, have been used to catalyze the CO₂ electrochemical reduction to formate [15, 20–30]. In this regard, Pb and Sn have been extensively studied. These catalysts are well-known for having high faradaic efficiencies (FEs) to formate, although they suffer from poor stability and high overpotentials, significantly hindering final applications [28, 31, 32].

Therefore, the development of highly active catalysts and the study of their mechanism for electrochemical reduction of CO₂ is an important issue to be solved in CO₂ reduction studies. By using metallic Bi as a catalyst, the overpotential for the electroreduction of CO₂ to formate can be reduced by 0.20–0.35 V. In a previous work we reported that nano-sized Bi deposited on a Cu foil can catalyze the reduction of CO₂ to formate at low overpotentials (0.99 V) and with high FE (91.3%) and good stability [33]. Electrochemical reduction of CO₂ to formic acid can be carried out with high FE (ca. 92%) at an overpotential of ca. 0.84 V over nano-Bi catalysts obtained by reduction of BiOCl nanosheets [34]. Qiao et al. reported that a micro-structured Bi catalyst can convert CO₂ to formate at low overpotentials (0.84 V) with a high FE of 90% [35]. A Bi nano-flower catalyst prepared by Qiu and co-workers [36] showed a maximum FE for producing formate of 99.2% at -1.5 V vs. saturated calomel electrode (SCE) while operating at a current density of 7.5 mA cm⁻².

Considering the above reports, Bi-based materials are promising catalysts for the reduction of CO₂ to formate. The influence of the morphology or the structure of the catalysts on their properties remains unclear. Therefore, it is necessary to study the structure–activity relationship of the Bi-based catalysts. In this work, we synthesized nano Bi₂O₂CO₃ and subsequently calcinated it at 300, 400, and 500 °C to form three different Bi₂O₃ samples. Since the active catalyst for the electrochemical reduction of CO₂ is Bi, the above materials were decorated on glass carbon electrodes (GCEs) and subsequently reduced to metallic Bi [37]. The performances of the four reduced Bi-based electrodes towards the electroreduction of CO₂ reduction were compared.

2. EXPERIMENTAL

2.1 Electrode preparation

A hydrothermal method was followed to successfully synthesize Bi₂O₂CO₃ microspheres (BOC) [38]. 2 mmol Bi(NO₃)₃·5H₂O and 1.5 mmol citric acid were dissolved in 10 mL of a 1 mol L⁻¹ HNO₃ solution with continuous stirring. Subsequently, a 2 mol L⁻¹ NaOH solution was added to adjust the pH to 4, and the as-obtained white-colored solution was transferred to an autoclave and left reacting at 180 °C for 24 h. The white product was collected by centrifugation, washed repeatedly with distilled water and absolute ethanol, and finally vacuum-dried at 60 °C for 5 h. The sphere-like BOC precursor was thermally treated in a furnace at 300, 400, and 500 °C for 3 h under air atmosphere to generate the Bi₂O₃-1, Bi₂O₃-2, and Bi₂O₃-3 samples, respectively.

20 mg of the as-prepared BOC or different Bi₂O₃ samples were firstly dissolved in 500 μL of ethanol. Then, 50 μL of a 5% Nafion solution was added to the above solution and subsequently sonicated for 20 min. 10 μL of the as-prepared sample solution was cast onto an L-style GCE (diameter 5 mm) and dried in air. Before each experiment, the GCE was polished with alumina powder, followed by sonication in deionized water and ethanol, and drying under nitrogen. The GCEs modified with the BOC and Bi₂O₃ precursors were reduced at -1.5 V vs. Ag/AgCl in a 0.1 mol L⁻¹ KHCO₃ aqueous solution for 10 min. After the reduction process, both the white precursor BOC and the yellow Bi₂O₃ samples all turned black. The reduced precursor BOC and the three Bi₂O₃ samples were labelled as r-BOC, r-Bi₂O₃-1, r-Bi₂O₃-2 and r-Bi₂O₃-3, respectively. The reduced electrodes were dried in air for 10 min before further experiments.

2.2 Electrochemical experiments

An undivided three-electrode glass cell containing 20 mL of electrolyte (0.1 mol L⁻¹ KHCO₃ aqueous solution) was used to carry out the electrochemical experiments. The working electrodes were GCEs modified with r-BOC, r-Bi₂O₃-1, r-Bi₂O₃-2 or r-Bi₂O₃-3. A Pt plate (2 cm²) and an Ag/AgCl electrode were chosen as the reference and the counter electrodes, respectively.

The electrochemical measurements were performed on a CHI 660E electrochemical workstation (Shanghai Chenhua Instruments Co., Ltd., China). Linear sweep voltammetry (LSV) was performed at a scan rate of 0.1 V s⁻¹ in N₂- or CO₂-saturated electrolytes prepared by bubbling with N₂ or CO₂ for 30

min. The current density was determined considering the area of the GCE. The electrolysis was carried out at a fixed negative potential for 10 C using a LAND CT2001C cell performance-testing instrument (Wuhan Electronics Co., Ltd., China). The electrolyte was saturated with CO₂ before the electrolysis experiments and was aerated with CO₂ continuously at a flow rate of 10 mL min⁻¹ during the electrolysis process.

2.3 Analysis and calculations

The scanning electron microscopy (SEM) images were obtained on a Hitachi S-4800 microscope. The X-ray diffraction (XRD) patterns were recorded on a Bruker D8 Advance powder X-ray diffractometer using Cu K α radiation (wavelength $\lambda = 0.15406$ nm). The formate accumulated in the electrolyte was directly analyzed by ion chromatography (Dionex ICS-5000⁺). The FE for producing formate was calculated by the following equation:

$$FE = \frac{2nF}{Q} \quad (1)$$

where n is the number of moles of the produced formate calculated according to IC data; F is the Faraday's constant (96485 C mol⁻¹); and Q is the total charge passed during the electrolysis ($Q = 10$ C herein).

3. RESULTS AND DISCUSSION

3.1 Catalysts characterization

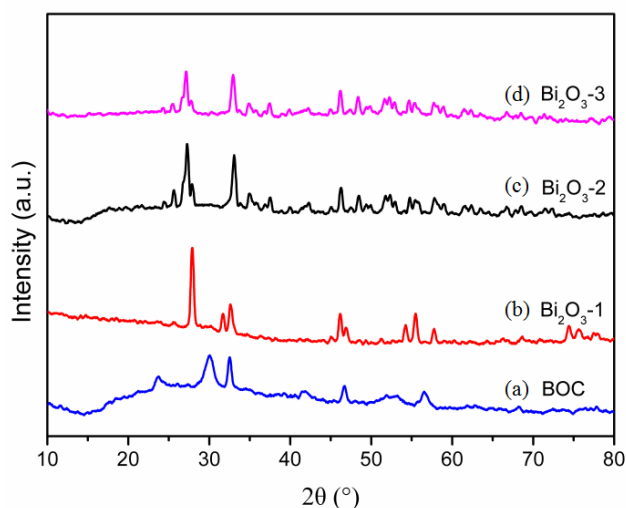


Figure 1. XRD patterns of the precursors: BOC (a), Bi₂O₃-1 (b), Bi₂O₃-2 (c), and Bi₂O₃-3 (d).

Fig. 1 reveals the phase and purity of the four synthesized samples by XRD. As can be seen in Fig. 1a, all the diffraction peaks of the BOC sample matched well with an hexagonal bismuth oxide carbonate phase Bi₂O₂CO₃ (JCPDS card No. 41-1488).

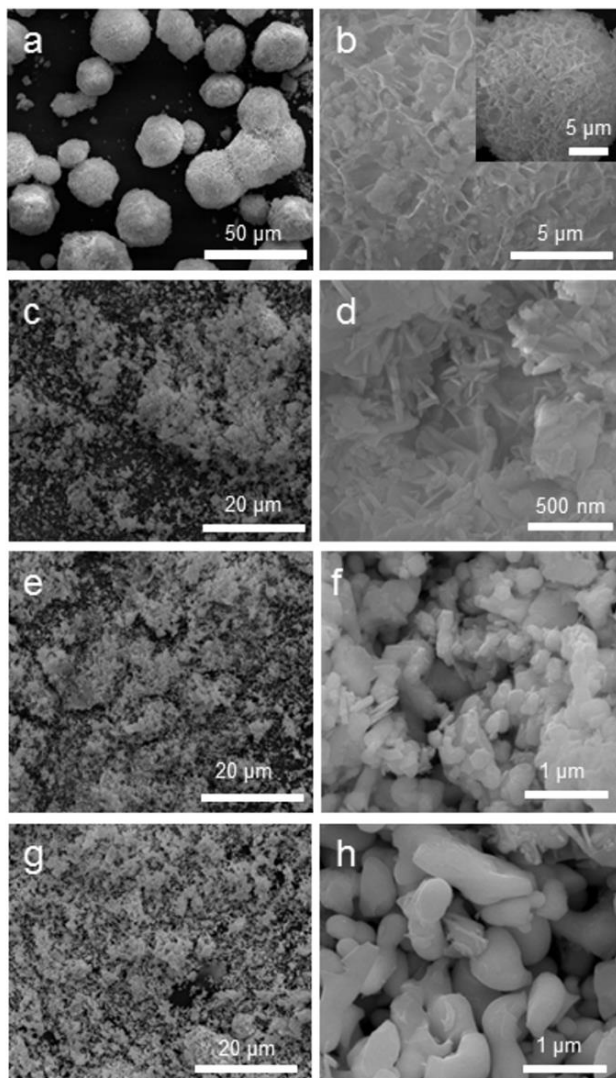
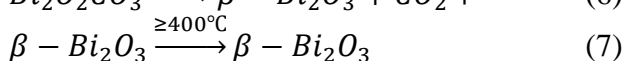
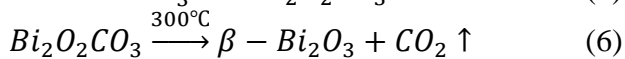
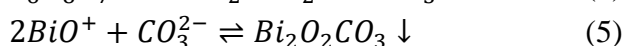
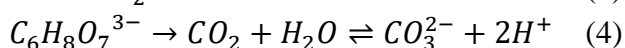
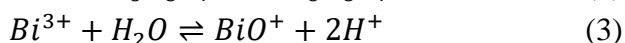
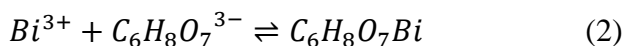


Figure 2. SEM images of the precursors: BOC (a, b), Bi₂O₃-1 (c, d), Bi₂O₃-2 (e, f), and Bi₂O₃-3 (g, h).

After calcination at 300 °C for 3 h, the XRD pattern showed peaks corresponding to tetragonal bismuth oxide (β -Bi₂O₃) (Fig. 1b), in line with the standard card (JCPDS card No. 27-0050). After calcination at 400 °C, β -Bi₂O₃ gradually turned into monoclinic α -Bi₂O₃ (JCPDS card No. 71-2274) (Fig. 1c). When the temperature of the thermal treatment reached 500 °C, a pure α -Bi₂O₃ phase was obtained (Fig. 1d). Tetragonal BOC was formed by a hydrothermal process (Eqs. 2–5) [39], while β -Bi₂O₃ (Eq. 6) and α -Bi₂O₃ (Eq. 7) were obtained by after calcination at 300–500 °C. In summary, the calcination temperature determined the chemical composition and phase structure of the synthesized samples.



The size and morphology of BOC and the rest of Bi₂O₃ samples were observed by SEM (Fig. 2). The left pictures correspond to low-magnification SEM images, while the right pictures correspond to high-magnification images. As shown in Fig. 2a, the BOC particles were spherical with an average diameter of ca. 22 μm. As shown in Fig. 2b, the BOC particles showed a porous structure composed of nanosheets on the surface of the particle. As shown in Figs. 2c–h, this spherical-like morphology changed after calcination. Calcination at 300 °C resulted in a morphological change for the β-Bi₂O₃ sample (Figs. 2c and d) from spherical to disordered thin nanosheets, revealing nanocrystals break off of the Bi₂O₃ spheres during the annealing process. When the annealing temperature exceeded 400 °C (Figs. 2e–h), nanocrystal aggregates formed larger particles and the thickness and size of the nanocrystals increasing, as revealed by the high magnification SEM images (Figs. 2f and h). These results suggested that the BOC nanosheets gradually transformed to β-Bi₂O₃ and α-Bi₂O₃ nanocrystals after the high-temperature treatment, and the overall flower-like microsphere morphology changed. The calcination temperature affects the morphology and phase structure of the sample. The catalysts prepared in this work were all metallic oxides easily reduced to metal at the reduction potential. Thus, BiOCl can be reduced to nano-sized Bi at potentials lower than −1.3 V vs. SCE, according to the report of Zhang et al. [34]. We used this method herein to reduce the four Bi-based samples to metal Bi, although the reduction potential was changed to −1.5 V vs. Ag/AgCl.

3.2 Catalytic performance measurements

Fig. 3 shows the current–time curves obtained during the electrochemical reduction of BOC, Bi₂O₃-1, Bi₂O₃-2, and Bi₂O₃-3 samples at a potential of −1.5 V for 10 min. As shown in the inset of Fig. 3a, while BOC was white, the three calcined Bi₂O₃ samples displayed different colors ranging from brilliant yellow to beige white as the calcination temperature increased (see the insets of Figs. 3b–d). This color change revealed that BOC gradually transformed to different crystal forms of Bi₂O₃ after the heat treatment. After the reduction process, BOC, Bi₂O₃-1, Bi₂O₃-2, and Bi₂O₃-3 on the GCEs turned black, which is the characteristic color of metallic Bi (see the insets of Fig. 3). Thus, we can ascertain whether oxidized Bi was reduced to metal Bi by the color changes of electrode before and after reduction. The reaction equation is:



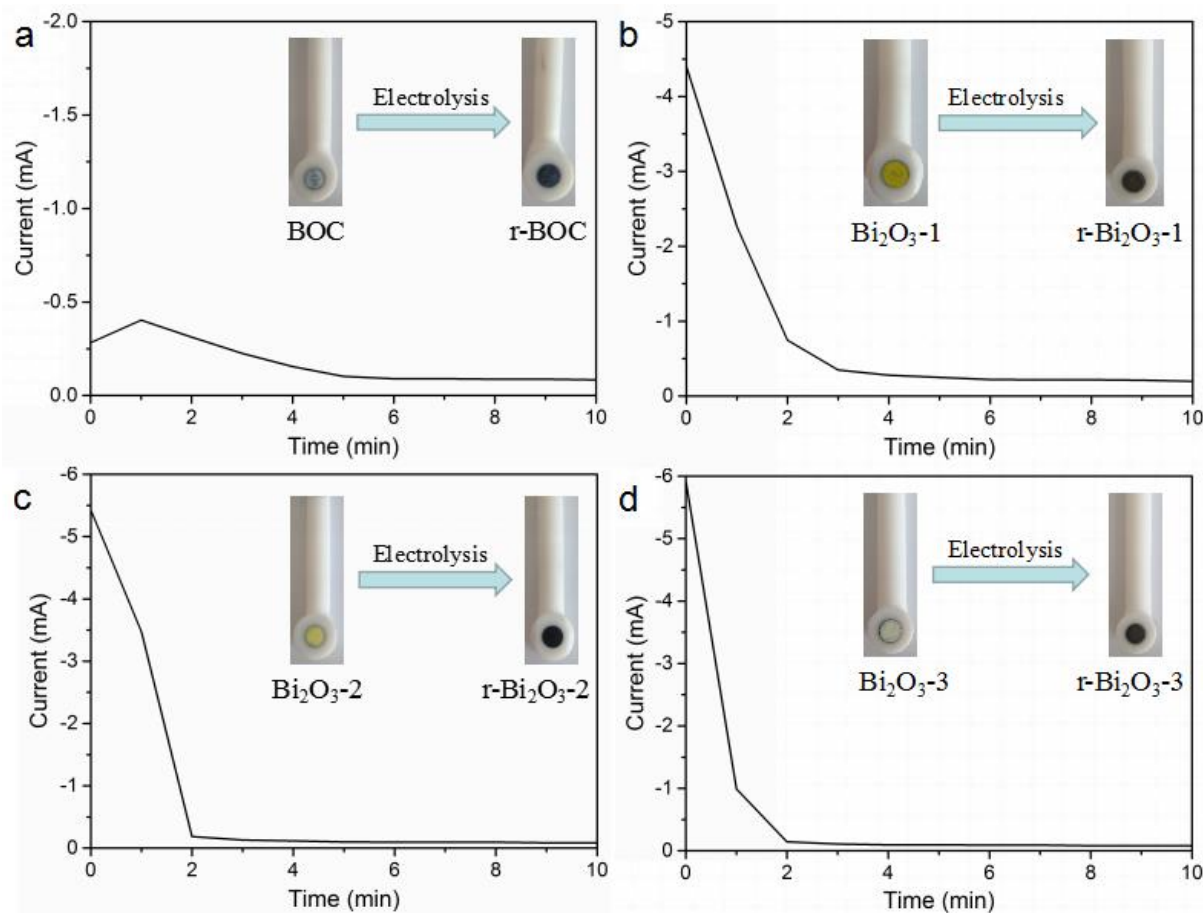


Figure 3. Current versus time during the electrochemical reduction of: BOC (a), Bi_2O_3 -1 (b), Bi_2O_3 -2 (c), and Bi_2O_3 -3 (d) at -1.5 V for 10 min. The insert images show pictures of the modified GCEs before and after the electrochemical reduction.

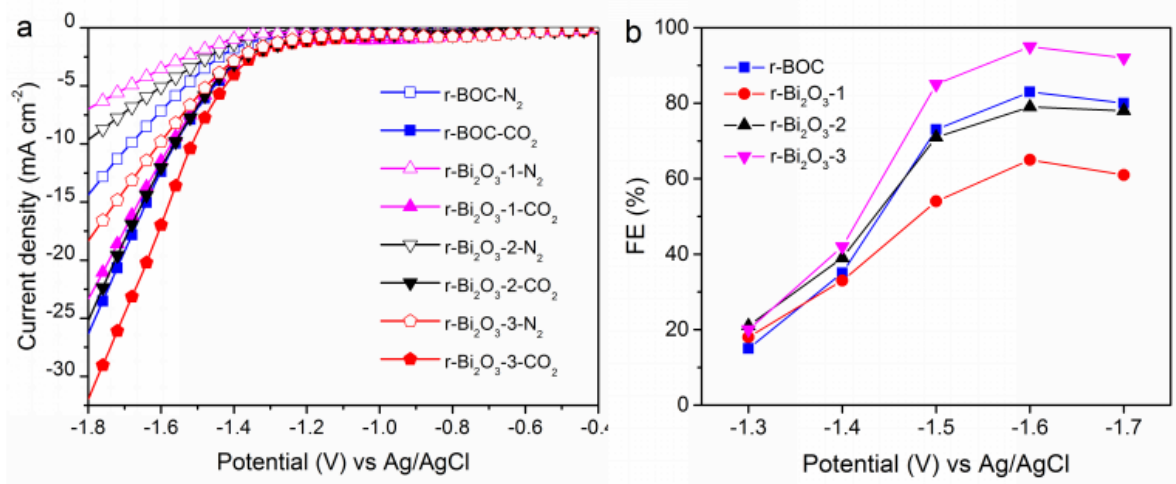


Figure 4. (a) LSV curves obtained on GCEs modified with r-BOC, r- Bi_2O_3 -1, r- Bi_2O_3 -2, and r- Bi_2O_3 -3 in N_2 - or CO_2 -saturated $0.1\text{ mol L}^{-1}\text{ KHCO}_3$ solutions. (b) FEs for producing formate on r-BOC, r- Bi_2O_3 -1, r- Bi_2O_3 -2, and r- Bi_2O_3 -3 at various electrolysis potentials.

The LSV curves showed by the GCEs modified with r-BOC, r-Bi₂O₃-1, r-Bi₂O₃-2 and r-Bi₂O₃-3 in N₂- and CO₂-saturated 0.1 mol L⁻¹ KHCO₃ solutions are compared in Fig. 4a. r-BOC-N₂ and r-BOC-CO₂ refers to the LSV curves obtained in N₂- and CO₂-saturated 0.1 mol L⁻¹ KHCO₃ solutions, respectively. The other curves are named according to the above rules. Regardless the electrolyte used, the current density increased significantly at cathodic end of the LSV curves. Under N₂, this enhanced current density was produced exclusively by the reduction of H₂O (hydrogen evolution reaction, HER, Eq. 9). Under CO₂, the current increase was produced by both the reduction of CO₂ and the HER:



All samples showed lower current densities under N₂ compared to CO₂. At a potential of -1.8 V, r-Bi₂O₃-3 showed the largest current density in the CO₂-saturated 0.1 mol L⁻¹ KHCO₃ solution (31.9 mA cm⁻²), followed by r-BOC, r-Bi₂O₃-2, and r-Bi₂O₃-1. The current density on r-Bi₂O₃-3 was higher than previous values reported in other literature. The tendency of the current density in the N₂-saturated electrolyte was consistent with that obtained under CO₂. Compared with other catalysts, r-Bi₂O₃-3 showed larger current density and more positive onset potentials in CO₂-saturated 0.1 mol L⁻¹ KHCO₃ solutions, suggesting that this sample possessed the highest activity and fastest reaction rate for CO₂ reduction among the materials tested herein.

Fig. 4b shows the FEs for producing formate on r-BOC, r-Bi₂O₃-1, r-Bi₂O₃-2, and r-Bi₂O₃-3 at various electrolysis potentials. The FEs of the four samples showed the same tendency. Thus, FE increased from -1.3 to -1.6 V because HER competed with the CO₂ electroreduction at a more negative potential. The FEs of all samples reached a maximum at -1.6 V. According to the following equation:

$$\eta = E^\circ - E(\text{vs. Ag/AgCl}) - 0.20 \text{ V} \quad (11)$$

we can obtain that the overpotential (η) is 0.99 V at -1.6 V. At this overpotential, the FEs for producing formate on r-BOC, r-Bi₂O₃-1, r-Bi₂O₃-2 and r-Bi₂O₃-3 were 83%, 65%, 79%, and 95%, respectively.

Fig. 5a depicts the electrolysis experiments over the r-BOC, r-Bi₂O₃-1, r-Bi₂O₃-2, and r-Bi₂O₃-3 electrodes in CO₂-saturated 0.1 mol L⁻¹ KHCO₃ solutions by applying a constant potential of -1.6 V for 10 C. The current did not decrease significantly with time. r-Bi₂O₃-3 showed the largest electrolysis current and the shortest electrolysis time. Thus, r-Bi₂O₃-3 showed the fastest reaction rate among the samples tested herein.

From the above experiments, we can conclude that pure α -Bi₂O₃ (r-Bi₂O₃-3) obtained by calcining BOC at 500 °C showed the best catalytic performance for the electrochemical reduction of CO₂ to formate. Therefore, we need to study the stability of this sample to ensure its practical applications. With this aim, we conducted 6 consecutive experiments at a potential of -1.6 V for 10 C, and the results are shown in Fig. 5b. It can be clearly seen that FE remained high for the 6 experiments (94–97%).

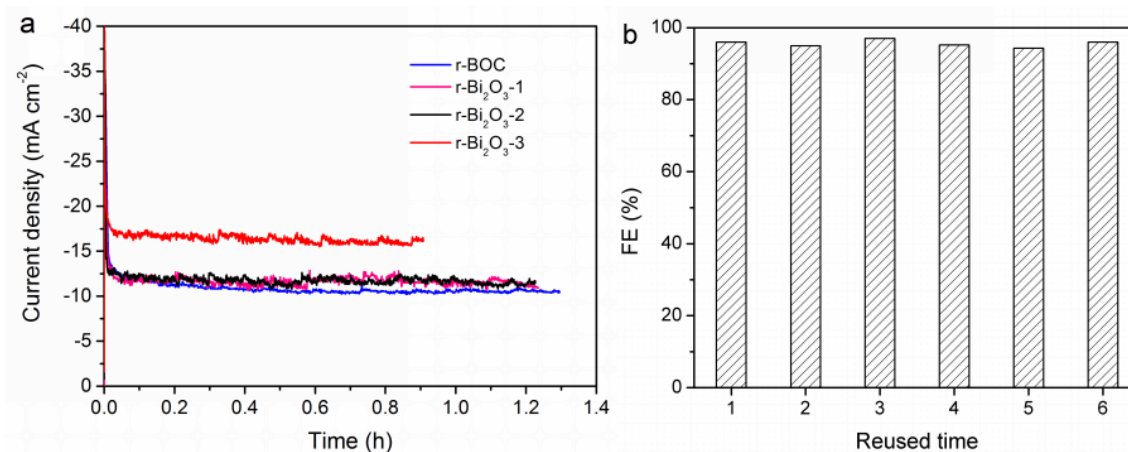


Figure 5. (a) Current–time curves of r-BOC, r-Bi₂O₃-1, r-Bi₂O₃-2, and r-Bi₂O₃-3 for the reduction of CO₂ at -1.6 V for 10 C. (b) Variations of the FEs for producing formate with the reused time of r-Bi₂O₃-3 modified GCE for six consecutive experiments at -1.6 V for 10 C.

3.3 Comparison of the catalytic performances

Table 1. Comparison of the catalytic performances of the four samples prepared herein and other electrocatalysts reported in literature for the reduction of CO₂ to formate.

Electrocatalyst	Overpotential (V)	FE (%)	Current density (mA cm ⁻²)	Ref
Sn plate	1.19	84.0	3.7	[40]
Porous Sn	1.19	91.5	7.4	[41]
Nanostructured Sn	1.15	93.6	10.2	[42]
Bi plate	0.95	51	2.1	[43]
Nano-sized Bi/Cu foil	0.89	15.2	1.9	[43]
Micro-structure Bi	0.99	94.0	4.6	[43]
Nano-flowered Bi	0.95	63	13.6	[35]
Bi nanoparticles	0.80	90	3.8	[36]
Nano-Bi obtained via reduction of BiOCl _{0.5} Br _{0.5}	0.83	99.2	7.5	[44]
Nano-sized Bi	0.83	94.7	3.3	[45]
Ultrathin Bi nanosheets	0.93	98.4	9.7	[46]
r-Bi ₂ O ₃ -3	0.89	84%	9.1	[47]
Oxygen vacancies-rich Co ₃ O ₄ single-unit-cell layers	0.68	95%	16	[48]
	0.99	95	17.0	This work

FE, current density, and overpotential are three equally important indicators to evaluate the performance of a CO₂ reduction catalyst. Among them, FE reflects the selectivity of the CO₂ reduction process towards the production of a determined product, the current density reflects the reaction rate of the CO₂ reduction reaction on the catalyst, and the overpotential reflects the energy consumption of the

catalyst conversion during CO₂ consumption. Most of the studies reported in the literature lack this analysis. We provided these three indicators for some related catalysts (Table 1) in order to compare the performance of the catalysts used herein with those of the catalysts reported in the literature. As shown in Table 1, the FE, current density, and overpotential of r-Bi₂O₃-3 (95%, 17 mA cm⁻², and 0.99 V, respectively) outperformed those of traditional Sn-based catalysts. Although some Bi-based catalysts showed a slightly lower overpotential and the oxygen vacancies-rich Co₃O₄ single-unit-cell layers showed an extremely low overpotential (0.22 V), r-Bi₂O₃-3 showed larger FE and current densities. By comparing the performance of the catalysts, we can conclude that r-Bi₂O₃-3 showed an excellent overall performance.

The most active Bi-based catalysts summarized in Table 1 were obtained by reducing a Bi-based oxide precursor. In this work, we found that the calcination temperature of the Bi₂O₃ precursor can affect the catalytic performance of resulting r-Bi₂O₃ CO₂ reduction catalysts. Increasing the calcination temperature from 300 to 500 °C resulted in larger catalytic activities over r-Bi₂O₃. The three r-Bi₂O₃ samples showed superior catalytic activities than r-BOC. According to the results of this work and those shown in Table 1, the performance towards the electrochemical reduction of CO₂ to formic acid varied greatly depending on the Bi-based catalyst used. Since the precursors used to prepare Bi-based oxides are diverse, we could not obtain the catalytic mechanism followed by the Bi-based catalysts, and additional work is necessary to obtain this mechanism.

4. CONCLUSION

In this work, a nano-precursor BOC has been synthesized by a hydrothermal method and subsequently calcinated at 300, 400, and 500 °C. The calcination temperature affected the morphology, the chemical composition, and phase structure of the prepared samples. As the temperature increased, the Bi₂O₃ particles agglomerated, resulting in larger particle sizes. The prepared BOC and the above calcinated materials were subsequently decorated on GCEs and then reduced to metal Bi. We compared the performance of the four reduced Bi-based electrodes towards the electroreduction of CO₂ to study the structure–activity relationship of the Bi-based catalysts. r-Bi₂O₃-3, prepared by calcination of BOC at 500 °C and subsequent reduction, showed an excellent performance towards the electrochemical reduction of CO₂ to formate compared to the rest of reduced samples. r-Bi₂O₃-3 showed a FE for producing formate as high as 95% at an overpotential of 0.99 V and with a current density is 17 mA cm⁻², outperforming most of the reported catalysts. Moreover, this FE remained stable (94–97%) after six consecutive experiments at –1.6 V for 10 C.

ACKNOWLEDGEMENTS

The work was supported by the National Natural Science Foundation of China (grant numbers 21603184, 21675139, 21575123).

References

1. D. Pletcher, *Electrochem. Commun.*, 61 (2015) 97-101.
2. CO₂ Earth, <https://www.co2.earth/>, (Accessed 5 July 2018).
3. A. Goepfert, M. Czaun, R. B. May, G. K. Prakash, G. A. Olah, S. R. Narayanan, *J. Am. Chem. Soc.*, 133 (2011) 20164-20167.
4. A. T. Najafabadi, *Int. J. Energ. Res.*, 37 (2013) 485-499.
5. A. D. Castillo, M. Alvarez-Guerra, A. Irabien, *AIChE J.*, 60 (2014) 3557-3564.
6. R. J. Lim, M. S. Xie, M. A. Sk, J. M. Lee, A. Fisher, X. Wang, K. H. Lim, *Catal. Today*, 233 (2014) 169-180.
7. Y. Y. Leea, H. S. Junga, J. M. Kimb, Y. T. Kang, *Appl. Catal. B-Environ.*, 224, (2018) 594-601.
8. S. J. Xie, Q. H. Zhang, G. D. Liu, Y. Wang, *Chem. Commun.*, 52 (2016) 35-59.
9. D. T. Whipple, P. J. A. Kenis, *J. Phys. Chem. Lett.*, 1 (2010) 3451-3458.
10. J. L. Qiao, Y. Y. L, F. Hong, J. J. Zhang, *Chem. Soc. Rev.*, 43 (2014) 631-675
11. D. R. Kauffman, J. Thakkar, R. Siva, C. Matranga, P. R. Ohodnicki, C. J. Zeng, R. C. Jin, *ACS Appl. Mater. Inter.*, 7 (2015) 15626-15632.
12. Z. Y. Sun, T. Ma, H. C. Tao, Q. Fan, B. Han, *Chem*, 3 (2017) 560-587.
13. H. Li, C. Oloman, *J. Appl. Electrochem.*, 36 (2006) 1105-1115.
14. D. W. Du, R. Lan, J. Humphreys, S. W. Tao, *J. Appl. Electrochem.*, 47 (2017) 661-678.
15. A. D. Castillo, M. Alvarez-Guerra, J. Solla-Gullón, A. Sáez, V. Montiel, A. Irabien, *J. CO₂ Util.*, 18 (2017) 222-228.
16. O. Scialdone, A. Galia, G. L. Nero, F. Proietto, S. Sabatino, B. Schiavo, *Electrochim. Acta*, 199 (2016) 332-341.
17. J. Eppinger, K. W. Huang, *ACS Energy Lett.*, 2 (2016) 188-195.
18. X. W. Yu, P. G. Pickup, *J. Power Sources*, 182 (2008) 124-132.
19. A. S. Agarwal, Y. M. Zhai, D. Hill, N. Sridhar, *ChemSusChem*, 4 (2011) 1301-1310.
20. C. H. Lee, M. W. Kanan, *ACS Catalysis*, 5 (2014) 465-469.
21. C. X. Zhao, Y. F. Bu, W. Gao, Q. Jiang, *J. Phys. Chem. C*, 121 (2017) 19767-19773.
22. R. L. Machunda, J. Lee, J. Lee, *Surf. Interface Anal.*, 42 (2010) 564-567.
23. Z. Xia, M. Freeman, D. X. Zhang, B. Yang, Dr. L. C. Lei, Dr. Z. J. Li, Dr. Y. Hou, *ChemElectroChem*, 5 (2018) 253-259.
24. P. Kang, C. Cheng, Z. F. Chen, C. K. Schauer, T. J. Meyer, M. Brookhart, *J. Am. Chem. Soc.*, 134 (2012) 5500-5503.
25. B. Schmid, C. Reller, S. S. Neubauer, M. Fleischer, R. Dorta, G. Schmid, *Catalysts*, 7 (2017) 161.
26. R. Reske, M. Duca, M. Oezaslan, K. J. P. Schouten, M. T. M. Koper, P. Strasser, *J. Phys. Chem. Lett.*, 4 (2013) 2410-2413.
27. Y. S. Fu, Y. N. Li, X. Zhang, Y. Y. Lin, X. D. Zhou, J. L. Qiao, *Chinese J. Catal.*, 7 (2016) 1081-1088.
28. C. C. Zhao, J. L. Wang, *Chem. Eng. J.*, 293 (2016) 161-170.
29. W. X. Lv, J. J. Bei, R. Zhang, W. J. Wang, F. Y. Kong, L. Wang, W. Wang, *ACS Omega*, 2 (2017) 2561-2567.
30. S. X. Wang, C. C. Jin, W. J. Qian, *J. Alloy. Compd.*, 615 (2014) 12-17.
31. V. S. K. Yadav, Y. Noh, H. Han, W. B. Kim, *Catal. Today*, 303 (2018) 276-281.
32. C. Oloman, H. Li, *ChemSusChem*, 1 (2008) 385-391.
33. W. X. Lv, J. Zhou, J. J. Bei, R. Zhang, F. Y. Kong, W. Wang, *Int. J. Electrochem. Sci.*, 11 (2016) 6183-6191.
34. H. Zhang, Y. Ma, F. J. Quan, J. J. Huang, F. L. Jia, L. Z. Zhang, *Electrochem. Commun.*, 46 (2014) 63-66.
35. X. Zhang, T. Lei, Y. Y. Liu, J. L. Qiao, *Appl. Catal. B-Environ.*, 218 (2017) 46-50.
36. Y. Qiu, J. Du, C. N. Dai, W. Dong, C. Y. Tao, *J. Electrochem. Soc.*, 165(2018) H594-H600.

37. R. Zhang, W. X. Lv, G. H. Li, L. X. Lei, *Mater. Lett.*, 141 (2015) 63-66.
38. G. Q. Zhu, J. Lian, M. Hojamberdiev, W. X. Que, *J. Clust. Sci.*, 24 (2013) 829-841.
39. R. P. Hu, X. Xiao, S. H. Tu, X. X. Zuo, J. M. Nan, *Appl. Catal. B-Environ.*, 163 (2015) 510-519.
40. R. Zhang, W. X. Lv, L. X. Lei, *Appl. Surf. Sci.*, 356 (2015) 24-29.
41. W. X. Lv, J. Zhou, F. Y. Kong, H. L. Fang, W. Wang, *Int. J. Hydrogen Energ.*, 41 (2016) 1585-1591.
42. S. Zhang, P. Kang, T. J. Meyer, *J. Am. Chem. Soc.*, 136 (2014) 1734-1737.
43. W. X. Lv, J. Zhou, J. J. Bei, R. Zhang, L. Wang, Q. Xu, W. Wang, *Appl. Surf. Sci.*, 393 (2017) 191-196.
44. X. Zhang, X. F. Hou, Q. Zhang, Y. X. Cai, Y. Y. Liu, J. L. Qiao, *J. Catal.*, 365 (2018) 63-70.
45. Y. Qiu, J. Du, C. N. Dai, W. Dong, C. Y. Tao, *J. CO₂ Util.*, 20(2017) 328-335.
46. J. J. Bei, R. Zhang, Z. D. Chen, W. X. Lv, W. Wang, *Int. J. Electrochem. Sci.*, 12 (2017) 2365-2375.
47. N. Han, Y. Wang, H. Yang, J. Deng, J. H. Wu, Y. F. Li, Y. G. Li, *Nat. commun.*, 9 (2018) 1320.
48. S. Gao, Z. T. Sun, W. Liu, X. C. Jiao, X. L. Zu, Q. T. Hu, Y. F. Sun, T. Yao, W. H. Zhang, S. Q. Wei, Y. Xie, *Nat. commun.*, 8 (2017) 14503.

© 2019 The Authors. Published by ESG (www.electrochemsci.org). This article is an open access article distributed under the terms and conditions of the Creative Commons Attribution license (<http://creativecommons.org/licenses/by/4.0/>).